LETTER

doi:10.1038/nature10344

Suppression of the coffee-ring effect by shape-dependent capillary interactions

Peter J. Yunker[1], Tim Still[1,2], Matthew A. Lohr[1] & A. G. Yodh[1]

When a drop of liquid dries on a solid surface, its suspended particulate matter is deposited in ring-like fashion. This phenomenon, known as the coffee-ring effect[1–3], is familiar to anyone who has observed a drop of coffee dry. During the drying process, drop edges become pinned to the substrate, and capillary flow outward from the centre of the drop brings suspended particles to the edge as evaporation proceeds. After evaporation, suspended particles are left highly concentrated along the original drop edge. The coffee-ring effect is manifested in systems with diverse constituents, ranging from large colloids[1,4,5] to nanoparticles[6] and individual molecules[7]. In fact—despite the many practical applications for uniform coatings in printing[8], biology[9,10] and complex assembly[11]—the ubiquitous nature of the effect has made it difficult to avoid[6,12–16]. Here we show experimentally that the shape of the suspended particles is important and can be used to eliminate the coffee-ring effect: ellipsoidal particles are deposited uniformly during evaporation. The anisotropic shape of the particles significantly deforms interfaces, producing strong interparticle capillary interactions[17–23]. Thus, after the ellipsoids are carried to the air–water interface by the same outward flow that causes the coffee-ring effect for spheres, strong long-ranged interparticle attractions between ellipsoids lead to the formation of loosely packed or arrested structures on the air–water interface[17,18,21,24]. These structures prevent the suspended particles from reaching the drop edge and ensure uniform deposition. Interestingly, under appropriate conditions, suspensions of spheres mixed with a small number of ellipsoids also produce uniform deposition. Thus, particle shape provides a convenient parameter to control the deposition of particles, without modification of particle or solvent chemistry.

A drop of evaporating water is a complex, difficult-to-control, non-equilibrium system. Along with capillary flow, the evaporating drop features an air–water interface shaped like a spherical cap and also Marangoni flows induced by small temperature differences between the top of the drop and the contact line[4]. Attempts to reverse or ameliorate the coffee-ring effect have thus far focused on manipulating capillary flows[6,12–16]. In this contribution, we show that uniform coatings during drying can be obtained simply by changing particle shape. The uniform deposition of ellipsoids after evaporation (Fig. 1a) is readily apparent, and stands in stark contrast to the uneven 'coffee ring' deposition of spheres (Fig. 1b) in the same solvent, with the same chemical composition, and experiencing the same capillary flows (Fig. 1c).

Much of the physics of the coffee-ring effect has been demonstrated with micrometre-sized polystyrene particles[1]. Here we also utilize such particles and simply modify their shape. Our experiments use water drops containing a suspension of micrometre-sized polystyrene spheres stretched asymmetrically to different aspect ratios[25,26]. We note that similar results were obtained for hydrophilic ellipsoids and other anisotropic particles (see Supplementary Fig. 4). We evaporate the drops on glass slides and study suspensions containing particles of the same composition, but with different major-axis/minor-axis aspect ratios (α), including spheres ($\alpha = 1.0$), slightly deformed spheres ($\alpha = 1.05, 1.1, 1.2, 1.5$) and ellipsoids ($\alpha = 2.5, 3.5$); we study volume fractions (ϕ) that vary from 10^{-4} to 2×10^{-1}.

During the drying process, the droplet contact line remains pinned in all suspensions, and fluid (carrying particles) flows outward from the drop centre to replenish the edges. Spherical particles are efficiently transported to the edge, either in the bulk or along the air–water interface, leaving a ring after evaporation is complete (Supplementary

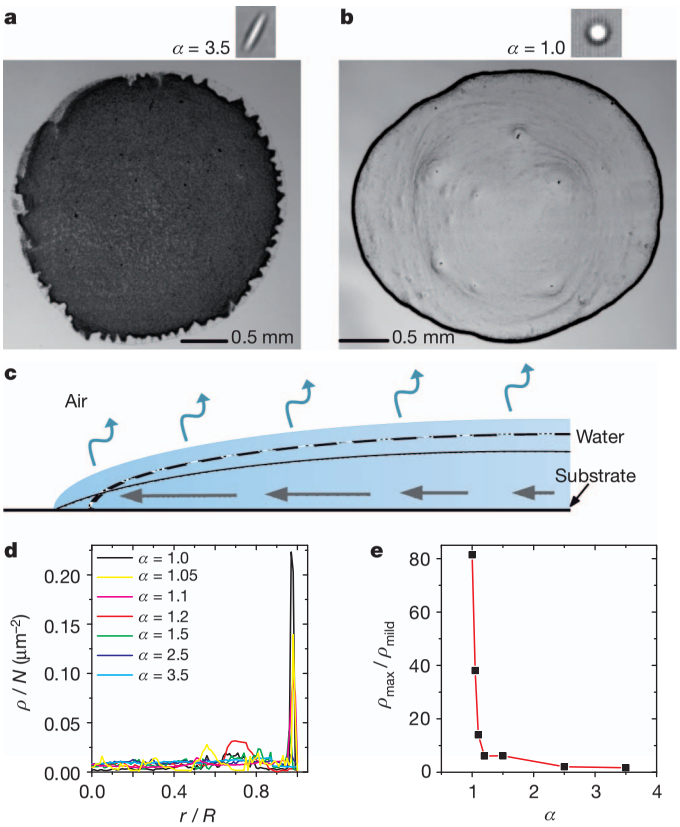

Figure 1 | Deposition of spheres and ellipsoids. **a**, **b**, Images of the final distributions of ellipsoids (**a**) and spheres (**b**) after evaporation. Insets, particle shape. **c**, Schematic diagram of the evaporation process, depicting capillary flow induced by pinned edges. Evaporation occurs over the entire drop surface (blue arrows), so if the contact line were free to recede, the drop profile would be preserved during evaporation (dashed line). However, the contact line remains pinned, so the contact angle decreases (solid line). Thus, a capillary flow (black arrows), from the drop's centre to its edges, is induced to replenish fluid at the contact line. **d**, Droplet-normalized particle number density, ρ/N, plotted as function of radial distance from centre of drop for ellipsoids with various major–minor axis aspect ratios (α). **e**, The maximum local density, ρ_{max}, normalized by the density in the middle of the drop, ρ_{mid}, plotted for all α. Red lines guide the eye.

[1]Department of Physics and Astronomy, University of Pennsylvania, Philadelphia, Pennsylvania 19104, USA. [2]Complex Assemblies of Soft Matter, CNRS-Rhodia-University of Pennsylvania UMI 3254, Bristol, Pennsylvania 19007, USA.

©2011 Macmillan Publishers Limited. All rights reserved

Movies 1, 3 and 5). Anisotropic particles ($\alpha > 1.0$), however, are only transported towards the edge until they reach the air–water interface (Supplementary Movies 2, 4 and 6). Once at that interface, ellipsoids experience strong long-ranged attractions to other ellipsoids[17–22], leading to the formation of loosely packed quasi-static or arrested structures at the interface[24]. On the interface, the interparticle attraction between anisotropic particles is more than two orders of magnitude stronger than the attraction between spheres[23]. Thus, anisotropic particles in these 'open' structures are strongly bound to each other and to the interface, so the energy cost of deforming, moving or breaking up these clusters is very large. As a result, ellipsoid mobility is markedly reduced, and they resist the radially outward flow (Supplementary Information). Thus, when evaporation is complete, anisotropic particles are much more uniformly deposited on the glass surface than spheres. Although spheres also adsorb onto the interface during evaporation, they do not significantly deform the interface[17]. Therefore, the radially outward fluid flow continues to push them to the drop's edge[4]. Figure 1 shows the final deposition, after evaporation on glass slides at 23 °C, of suspensions of particles ($\phi = 0.005$, 1 μl) with different aspect ratios. Spherical particles are primarily deposited at the original perimeter of the droplet (Fig. 1b). Ellipsoidal particles are distributed much more uniformly (Fig. 1a).

To quantify the behaviour shown qualitatively in Fig. 1a and b, we determined the areal number fraction, $\rho(r)$, of particles deposited as a function of radial distance (r) from the drop centre, normalized by the number of particles, N (Fig. 1d). For spheres ($\alpha = 1.0$), ρ/N is ~70 times larger at $r/R \approx 1$ than in the middle of the drop (here R is the drop radius). Conversely, the density profile of ellipsoidal particles is fairly uniform as a function of r/R. As aspect ratio is increased from unity, the peak at large r/R decreases. A clear coffee-ring effect persists for particles only marginally distorted from their original spherical shape ($\alpha = 1.05$ and 1.1), but particles slightly more anisotropic ($\alpha = 1.2$) are deposited uniformly. This behaviour is summarized by calculating ρ_{max}/ρ_{mid} (Fig. 1e), where ρ_{max} is the maximum value of ρ (typically located at $r/R \approx 1$) and ρ_{mid} is the average value of ρ in the middle of the drop ($r/R < 0.25$). (See Supplementary Information and Supplementary Fig. 6.)

Quantification of the spatio-temporal evaporation profile of the suspensions provides a first step towards understanding why ellipsoids are deposited uniformly. We measure drop mass of different suspensions during evaporation (Supplementary Fig. 1). The drop mass decreases linearly in time, and the mass rate-of-change (10.0 μg s^{-1}) is the same for drops of sphere suspension, drops of ellipsoid suspension, and drops of pure water[1,5].

To confirm that the contact line remains pinned until the final stage of evaporation, we used video microscopy to measure drop radius during evaporation (Supplementary Fig. 2). Using these data, the time at which evaporation finishes, t_{final}, is readily identified as the time when the drop radius shrinks to zero. Interestingly, we find that the radius decreases by less than 10% until $t = 0.8t_{final}$; that is, the contact line is pinned for the vast majority of the evaporation time period in all samples. For suspensions of ellipsoids, the contact line becomes partially depinned around $t = 0.7t_{final}$, but does not become completely depinned until $t = 0.8t_{final}$. The experiments thus demonstrate that despite similar contact line behaviour, capillary flow, and evaporation rates, the deposition of spheres and ellipsoids differs significantly.

Experimental images clearly reveal that whereas spheres are carried to the drop's edge (Fig. 2a–d), ellipsoids are carried there to far lesser degree (Fig. 2e–h) (Supplementary Movies 2 and 4). We measured the average areal particle density close to the contact line, $\rho_R = \int_{r=R-20\mu m}^{r=R} \rho(r)dr$, as a function of time (Fig. 2i), and thereby demonstrated that ellipsoid density grows at a slower rate than sphere density (Supplementary Information.)

Images of particles near the drop's contact line (Fig. 2j–m) reveal that unlike spheres, which are carried from the bulk all the way to the contact line, most ellipsoids adhere to the loosely packed structures at

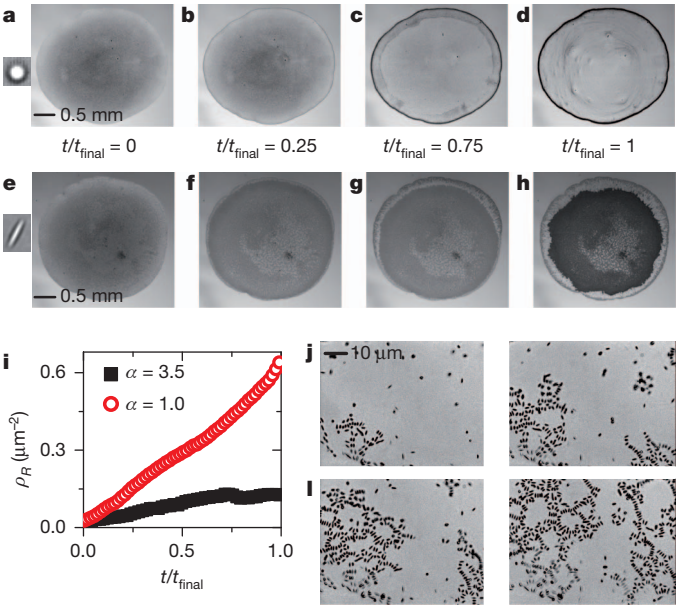

Figure 2 | Transportation of particles over time. **a–h**, Experimental snapshots at different times t/t_{final} during the evaporation of a drop of particle suspension; shown are data for spherical particles (left inset: **a–d**) and for ellipsoidal particles with aspect ratio $\alpha = 3.5$ (left inset: **e–h**). **i**, The areal particle density, ρ_R, located within 20 μm of the contact line (that is, the drop edge) as a function of time during evaporation for ellipsoidal particles. **j–m**, Images of the assembly of ellipsoids at the air–water interface over the same time intervals during evaporation. Loosely packed structures form on the air–water interface, preventing ellipsoids from reaching the edge. The three-phase contact line is at the bottom left corner of these snapshots.

the air–water interface before they reach the contact line (see below). This capillary attraction has been characterized in prior experiments as long-ranged and very strong[17,18,23,27–29]. The loosely packed configurations formed by ellipsoids on the interface are structurally similar to those seen in previous experiments on ellipsoids at flat air–water and water–oil interfaces[17,18,21]. They produce a surface viscosity that is much larger than the bulk viscosity, facilitating ellipsoid resistance to radially outward flows (Supplementary Information). We note that spheres also adsorb onto the interface during evaporation. However, spheres do not strongly deform the interface[17] and they experience a much weaker interparticle attraction than ellipsoids[23]; thus, radially outward fluid flows push spheres to the drop's edge[4].

Snapshots of the region within 40 μm of the drop contact line confirm that whereas spheres pack closely at the edge (Fig. 3a), ellipsoids form loosely packed structures (Fig. 3b), which prevent particles from reaching the contact line (Supplementary Movies 5 and 6). Particles with $\alpha = 1.2$ and 1.5 pack at higher area fractions than ellipsoids with $\alpha > 1.5$, resulting in larger values of ρ_{max}/ρ_{mid} for $\alpha = 1.2$ and 1.5 and producing the small peak in $\rho(r)$ at $r/R = 0.7$ for $\alpha = 1.2$. The structures on the air–water interface appear to be locally arrested or 'jammed'[24], that is, particles do not rearrange. Once an ellipsoid joins a collective structure, its position relative to other ellipsoids changes by less than 20 nm (the lower limit of our resolution), and the structure only rearranges when new particles become attached to the interface. In order to quantify the ability of interfacial aggregates of ellipsoids to resist bulk flow, we calculated the Boussinesq number for our experimental system (see Supplementary Information for details), that is, the ratio of the surface drag to bulk drag for ellipsoids with $\alpha = 3.5$. The calculated Boussinesq number is much greater than 1, and grows exponentially with time (Supplementary Fig. 3). This behaviour is expected, as shear stress grows linearly with particle velocity, but elastic modulus grows exponentially with ellipsoid area fraction[21], and dominates the ratio. As might be anticipated, the Boussinesq number for spheres was much smaller than for ellipsoids, that is, it is less than 1.

©2011 Macmillan Publishers Limited. All rights reserved

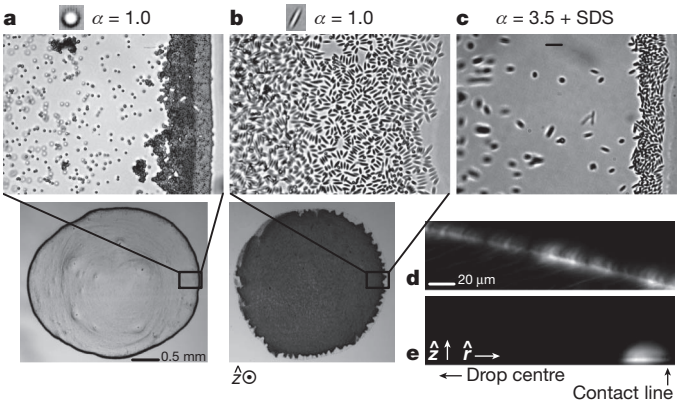

Figure 3 | High-magnification images of particles near the drop contact line. a–c, Top, microscope images of a region within 40 μm of the drop contact line, taken at time $t/t_{final} = 0.5$, for suspensions of spheres (**a**), ellipsoids ($\alpha = 3.5$) (**b**), and ellipsoids ($\alpha = 3.5$) mixed with surfactant (SDS; 0.2 wt%) (**c**). Spheres pack closely at the contact line. Ellipsoids form loosely packed structures. Surfactant lowers the drop surface tension, making ellipsoids pack closely at the contact line. For **a** and **b**, pictures of the entire drop after evaporation are shown (bottom) and the magnified region is boxed. **d**, **e**, Confocal projections of suspensions of ellipsoids ($\alpha = 2.5$) (**d**) and spheres (**e**) onto the z–r plane in cylindrical coordinates. This z-direction is indicated below **b**.

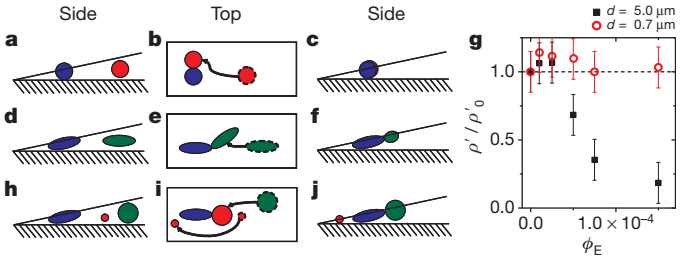

Figure 4 | Behaviour of spheres, ellipsoids, and mixtures of spheres and ellipsoids in drying liquid drops. For all cartoons, the leftmost and rightmost panels are side views at early and late times, respectively, and the centre panel is a top view showing particle trajectories (arrows) linking those times (original positions indicated with dashed lines, final positions indicated with solid lines). **a–f**, Cartoons depicting capillary flow that carries spheres (**a–c**) and ellipsoids (**d–f**) to the drop's edge. Spheres leave a ring-like formation, whereas ellipsoids form loosely packed structures on the air–water interface. **g**, The deposition of mixtures of spheres and ellipsoids is characterized by the ratio $\rho' = \rho_{max}/\rho_{mid}$ (where ρ_{max} is the maximum local density and ρ_{mid} is the density in the middle of the drop) as a function of ellipsoid volume fraction, ϕ_E. Two sizes of particles are studied: $d = 5.0$ μm (black squares) and $d = 0.7$ μm (red circles), where d is the particle diameter. ρ' is normalized by ρ'_0, the value of ρ' when there are no ellipsoids present, that is, when $\phi_E = 0$. The dashed line represents no change in the distribution of particles. The coffee-ring effect persists for mixtures of small spheres and ellipsoids, but is destroyed for mixtures of large spheres and ellipsoids. Error bars represent the uncertainty that results from finite bin sizes. **h–j**, Cartoons depicting capillary flow that carries suspensions of spheres and ellipsoids to the drop's edge.

To confirm that deformations of the interface are responsible for the uniform deposition of ellipsoids, we added a small amount of surfactant (sodium dodecyl sulphate, SDS, 0.2% by weight) to a suspension of ellipsoids with $\alpha = 3.5$. Surfactant lowers the surface tension of the drop, thus making interfacial deformations less energetically costly and shorter-range. This restores the coffee-ring effect; ellipsoids pack closely at the contact line (Fig. 3c), in a manner similar to spheres (Supplementary Movie 7). The ellipsoids no longer strongly deform the air–water interface and their interactions with other ellipsoids are correspondingly reduced; as a result, they move more easily along and on-and-off the interface and are able to pack close to the contact line. (We note that, without added surfactant, ellipsoids increase the air–water surface tension, as evidenced by an increase in contact angle from ~15° for spheres to ~35° for ellipsoids with $\alpha = 3.5$; Supplementary Fig. 5).

We obtained direct evidence that the ellipsoids sit at the air–water interface, using three-dimensional confocal microscopy. Confocal snapshots, projected onto a side view of the drop, clearly confirm that ellipsoids sit at the air–water interface (Fig. 3d), whereas spheres do not and are carried all the way to the contact line (Fig. 3e, summarized in Fig. 4a–f).

Finally, we showed that the addition of small numbers of ellipsoids to sphere suspensions can also destroy the coffee-ring effect. If the diameter of the spheres is smaller than the minor axis of the ellipsoids, then the coffee ring persists; if the diameter is larger than that axis, then the coffee ring is destroyed. To observe this effect, we evaporated drops of suspensions containing both ellipsoids and spheres.

Each suspension contains ellipsoids with $\alpha = 3.5$, stretched from particles of diameter $d = 1.3$ μm, and spheres suspended at a volume fraction $\phi = 0.02$. Evaporative deposits are characterized as a function of ellipsoid volume fraction ϕ_E via $\rho'(\phi_E) = \rho_{max}/\rho_{mid}$ (Fig. 4g). First, we evaporated suspensions containing smaller spheres with $d = 0.7$ μm, along with the ellipsoids at volume fractions ranging from $\phi_E = 0$ to 1.5×10^{-4}. After evaporation, the spheres displayed a clear coffee ring, and this coffee ring persists even if more ellipsoids are added to the initial suspension (Fig. 4g). The coffee-ring effect is uninhibited because spheres that are smaller than the ellipsoids are easily able to move under or through the loosely packed particle structures and reach the drop's edge (Fig. 4h–j).

If, instead, we evaporate suspensions containing larger spheres with $d = 5.0$ μm, along with the same ellipsoids at the same volume fractions used previously, then different phenomena emerge. When the ellipsoid volume fraction is very small ($\phi_E \leq 2.5 \times 10^{-5}$), the suspensions still exhibit a clear coffee-ring effect. However, at larger ϕ_E, the coffee ring is diminished, and it eventually disappears at sufficiently large ϕ_E, that is, $\phi_E \approx 1.5 \times 10^{-4}$ (Fig. 4g). In this case, the larger spheres adsorb onto the air–water interface farther from the drop edge than do the ellipsoids. In the absence of ellipsoids, the spherical particles form closely packed aggregates, but in the presence of ellipsoids they instead join the loosely packed aggregates, eliminating the coffee-ring effect (Fig. 4h–j). Thus, uniform depositions can potentially be made with existing suspensions, simply by adding ellipsoids.

Looking forward, we note that the ability to deposit particles uniformly is desirable in many applications[8]. Unfortunately, most proposed methods for avoiding the coffee-ring effect require long multistage processes, which can be costly in manufacturing or require use of organic solvents which are sometimes flammable and toxic[6,12]. Here we have shown that by exploiting a particle's shape, a uniform deposit can be easily derived from an evaporating aqueous solution. These results further suggest that other methods of inducing strong capillary interactions, for example, surface roughness[30], may also produce uniform deposits.

METHODS SUMMARY

To create ellipsoidal particles, 1.3-μm-diameter polystyrene particles (Invitrogen) are suspended in a polyvinyl alcohol (PVA) gel and are heated above the polystyrene melting point (~100 °C), but below the PVA melting point (~180 °C)[25,26]. Polystyrene melts in the process, but the PVA gel only softens. The PVA gel is then pulled so that the spherical cavities containing liquid polystyrene are stretched into ellipsoidal cavities. When the PVA gel cools, polystyrene solidifies in the distorted cavities and becomes frozen into an ellipsoidal shape. The hardened gel is dissolved in water, and the PVA is removed via centrifugation (see Supplementary Information for more details about PVA removal). Each iteration of this process creates ~10^9 ellipsoidal particles in ~50-μl suspensions. The particles are charge-stabilized, and the resultant suspensions are surfactant-free. Snapshots of experimental particles are shown in Fig. 1a and b insets. The aspect ratio polydispersity is ~10%. To ensure the preparation process does not affect particle deposition, our spheres undergo the same procedure, without stretching. In our experiments, suspensions of particles are placed on glass slides (Fisher Scientific) and evaporated.

Confocal snapshots are shown in Fig. 3d and e. By integrating the brightness of each pixel over a period of 0.05 s, only particles that are roughly stationary during

©2011 Macmillan Publishers Limited. All rights reserved

this time period appear in the images. Snapshots are then projected onto a side-view of the drop.

Received 12 April; accepted 4 July 2011.

1. Deegan, R. D. *et al.* Capillary flow as the cause of ring stains from dried liquid drops. *Nature* **389,** 827–829 (1997).
2. Denkov, N. D. *et al.* Two-dimensional crystallization. *Nature* **361,** 26 (1993).
3. Hu, H. & Larson, R. G. Evaporation of a sessile droplet on a substrate. *J. Phys. Chem. B* **106,** 1334–1344 (2002).
4. Deegan, R. D. *et al.* Contact line deposits in an evaporating drop. *Phys. Rev. E* **62,** 756–765 (2000).
5. Deegan, R. D. Pattern formation in drying drops. *Phys. Rev. E* **61,** 475–485 (2000).
6. Bigioni, T. P. *et al.* Kinetically driven self assembly of highly ordered nanoparticle monolayers. *Nature Mater.* **5,** 265–270 (2006).
7. Kaya, D., Belyi, V. A. & Muthukumar, M. Pattern formation in drying droplets of polyelectrolyte and salt. *J. Chem. Phys.* **133,** 114905 (2010).
8. Park, J. & Moon, J. Control of colloidal particle deposit patterns within picoliter droplets ejected by ink-jet printing. *Langmuir* **22,** 3506–3513 (2006).
9. Dugas, V. Immobilization of single-stranded DNA fragments to solid surfaces and their repeatable specific hybridization: covalent binding or adsorption? *Sens. Actuators B* **101,** 112–121 (2004).
10. Dugas, V., Broutin, J. & Souteyrand, E. Droplet evaporation study applied to DNA chip manufacturing. *Langmuir* **21,** 9130–9136 (2005).
11. de Gans, B. J., Duineveld, P. C., & Schubert, U. S. Inkjet printing of polymers: state of the art and future developments. *Adv. Mater.* **16,** 203–213 (2004).
12. Hu, H. & Larson, R. G. Marangoni effect reverses coffee-ring depositions. *J. Phys. Chem. B* **110,** 7090–7094 (2006).
13. Weon, B. M. & Je, J. H. Capillary force repels coffee-ring effect. *Phys. Rev. E* **82,** 015305 (2010).
14. Kajiya, T., Kobayashi, W., Okuzono, T. & Doi, M. Controlling the drying and film formation processes of polymer solution droplets with addition of small amount of surfactants. *J. Phys. Chem. B* **113,** 15460–15466 (2009).
15. Nguyen, V. X. & Stebe, K. J. Patterning of small particles by a surfactant-enhanced Marangoni-Benard instability. *Phys. Rev. Lett.* **88,** 164501 (2002).
16. Park, B. J. & Furst, E. M. Fluid-interface templating of two-dimensional colloidal crystals. *Soft Matter* **6,** 485–488 (2010).
17. Loudet, J. C., Yodh, A. G. & Pouligny, B. Wetting and contact lines of micrometer-sized ellipsoids. *Phys. Rev. Lett.* **97,** 018304 (2006).
18. Loudet, J. C., Alsayed, A. M., Zhang, J. & Yodh, A. G. Capillary interactions between anisotropic colloidal particles. *Phys. Rev. Lett.* **94,** 018301 (2005).
19. Bowden, N., Arias, F., Deng, T. & Whitesides, G. M. Self-assembly of microscale objects at a liquid/liquid interface through lateral capillary forces. *Langmuir* **17,** 1757–1765 (2001).
20. Brown, A. B. D., Smith, C. G. & Rennie, A. R. Fabricating colloidal particles with photolithography and their interactions at an air-water interface. *Phys. Rev. E* **62,** 951–960 (2000).
21. Madivala, B., Fransaer, J. & Vermant, J. Self-assembly and rheology of ellipsoidal particles at interfaces. *Langmuir* **25,** 2718–2728 (2009).
22. Madivala, B., Vandebril, S., Fransaer, J. & Vermant, J. Exploiting particle shape in solid stabilized emulsions. *Soft Matter* **5,** 1717–1727 (2009).
23. Park, B. J. & Furst, E. M. Attractive interactions between colloids at the oil-water interface. *Soft Matter* http://dx.doi.org/10.1039/c1sm00005e (published online, 26 April 2011).
24. Fournier, J. B. & Galatola, P. Anisotropic capillary interactions and jamming of colloidal particles trapped at a liquid-fluid interface. *Phys. Rev. E* **65,** 031601 (2002).
25. Champion, J. A., Katare, Y. K. & Mitragotri, S. Making polymeric micro- and nanoparticles of complex shapes. *Proc. Natl Acad. Sci. USA* **104,** 11901–11904 (2007).
26. Ho, C. C., Keller, A., Odell, J. A. & Ottewill, R. H. Preparation of monodisperse ellipsoidal polystyrene particles. *Colloid Polym. Sci.* **271,** 469–479 (1993).
27. Lehle, H., Noruzifar, E. & Oettel, M. Ellipsoidal particles at fluid interfaces. *Eur. Phys. J. E* **26,** 151–160 (2008).
28. Lewandowski, E. P., Bernate, J. A., Tseng, A., Searson, P. C. & Stebe, K. J. Oriented assembly of anisotropic particles by capillary interactions. *Soft Matter* **5,** 886–890 (2009).
29. Danov, K. D. & Kralchevsky, P. A. Capillary forces between particles at a liquid interface: general theoretical approach and interactions between capillary multipoles. *Adv. Colloid Interface Sci.* **154,** 91–103 (2010).
30. Stamou, D., Duschl, C. & Johannsmann, D. Long-range attraction between colloidal spheres at the air-water interface: the consequence of an irregular meniscus. *Phys. Rev. E* **62,** 5263–5272 (2000).

Supplementary Information is linked to the online version of the paper at www.nature.com/nature.

Acknowledgements We thank K. B. Aptowicz, A. Basu, E. Buckley, J. C. Crocker, P. Habdas, T. Lubensky and K. J. Stebe for discussions and critical reading of the manuscript. We thank J. Crassous and H. Dietsch for the hydrophilic ellipsoids and spheres (see Supplementary Fig. 4). We acknowledge financial support from the National Science Foundation through DMR-0804881, the PENN MRSEC DMR-0520020 and NASA NNX08A00G. T.S. thanks DAAD for a postdoctoral fellowship.

Author Contributions P.J.Y. initiated the research, designed and performed the experiments, synthesized the colloidal particles, and analysed the data with support from A.G.Y., T.S. and M.A.L.; P.J.Y. and A.G.Y. wrote the manuscript, with support from T.S. and M.A.L.

Author Information Reprints and permissions information is available at www.nature.com/reprints. Readers are welcome to comment on the online version of this article at www.nature.com/nature. The authors declare competing financial interests: details accompany the full-text HTML version of the paper at www.nature.com/nature. Correspondence and requests for materials should be addressed to P.J.Y. (pyunker@sas.upenn.edu).

©2011 Macmillan Publishers Limited. All rights reserved